

## Near infrared down-conversion luminescence of $\text{Ba}_4\text{Y}_3\text{F}_{17}:\text{Yb}^{3+}:\text{Eu}^{3+}$ nanoparticles under ultraviolet excitation

S. V. Kuznetsov<sup>1\*</sup>, A. S. Nizamutdinov<sup>2</sup>, E. I. Madirov<sup>2</sup>, V. V. Voronov<sup>1</sup>, K. S. Tsoy<sup>2</sup>, A. R. Khadiev<sup>2</sup>,  
A. D. Yaprntsev<sup>3</sup>, V. K. Ivanov<sup>3</sup>, S. S. Kharintsev<sup>2</sup>, V. V. Semashko<sup>2</sup>

<sup>1</sup>Prokhorov General Physics Institute of the Russian Academy of Sciences, Russia

<sup>2</sup>Kazan Federal University, Russia

<sup>3</sup>Kurnakov Institute of General and Inorganic Chemistry of the Russian Academy of Sciences, Russia

\*kouznetzovsv@gmail.com

PACS 42.70.-a, 81.20.Fw

DOI 10.17586/2220-8054-2020-11-3-316-323

The single-phase solid solutions  $\text{Ba}_4\text{Y}_3\text{F}_{17}:\text{Yb}:\text{Eu}$  with fluorite-type structure were synthesized by co-precipitation from aqueous solution technique. The average particle size was approximately 100 nm without agglomeration. The sensitized down-conversion luminescence of  $\text{Yb}^{3+}$  ions was observed under 296 nm excitation. The quantum yield of  $\text{Yb}^{3+}$  luminescence was found to reach a value of 0.4 % for samples with Eu/Yb ratios of 0.1/1.0 and 0.1/10.0.

**Keywords:** nanofluoride, down-conversion, luminescence.

*Received: 16 April 2020*

### 1. Introduction

According to the International Energy Agency (IEA) and the European Environment Agency (EEA), the energy consumption increases from year to year. It stimulates the search for new sources of energy and improving the efficiency of existing ones. According to the forecast, the terawatt energy will be generated by means of photovoltaic devices until 2030 years with a simultaneous reduction of kW/h cost [1]. One of the most affordable source of energy is solar energy. Silicon-based solar cells are mostly used for solar energy utilization. Most of this energy will be generated by silicon solar panels. In addition to silicon, various multilayer compositions such as GaAs, CdTe, Cu(In,Ga)Se<sub>2</sub>, and recently proposed perovskite structures [2, 3]. The latter are expensive and difficult to produce on an industrial scale. Additionally, there is the problem to dispose them after the expiration due to toxic components and use of such compositions is contrary to the principles of green chemistry. The advantages of silicon are chemical availability and the maturity of the technological chains, the disposal of electronic components, including those containing rare-earth elements.

At the same time, one serious drawback of silicon-based solar cells is relatively low light-to-electrical energy conversion efficiency (LECE), namely, no higher than 25 % for the best samples [4, 5]. The region of the highest photosensitivity of silicon is located about 1  $\mu\text{m}$  and his LECE spectrum poorly corresponds the solar emission spectrum.

The enhancement of silicon solar panels efficiency by down-conversion of solar irradiation from ultraviolet and blue spectral range to the 1  $\mu\text{m}$  spectral range is an urgent task and it is extremely actual for space applications [6–9]. Prospective emitter is trivalent ytterbium ion due to near-infrared (NIR) luminescence band around 1000 nm ( $^2\text{F}_{5/2}-^2\text{F}_{7/2}$  transition) [9–13], which well coincides with the top of LECE spectrum of silicon batteries. One of the new thoroughly investigated luminescence matrices is  $\text{Ba}_4\text{Y}_3\text{F}_{17}$  [14–17], because it demonstrated the high quantum yield of down-conversion luminescence [14].

Energy transfer from the UV and blue spectral regions to ytterbium is possible for various sensitizing cations absorbing in these spectral regions. One especially efficient mechanism of energy transfer is through stepwise relaxation of a sensitizer ion, resulting in the excitation of two acceptor ions by quantum cutting mechanism [12, 13, 18, 19]. The quantum cutting demonstrated high quantum efficiency coefficient up to 195 % but the quantum yield of NIR luminescence is low. A more efficient pathway is simple downshifting in a systems with higher quantum yield of luminescence. A promising composition is Yb/Eu doping pair, because absorption spectrum of europium comprises several lines in the UV and blue spectral regions. The highest directly measured quantum yield of ytterbium luminescence (2.5 %) upon 266 nm pumping was reached for the  $\text{SrF}_2:\text{Yb}$  (1.0 mol %):Eu (0.05 mol %) powder [20].

The purpose of this paper is to synthesize  $\text{Ba}_4\text{Y}_3\text{F}_{17}:\text{Yb}:\text{Eu}$  solid solution and to study its luminescent properties. This specimen of interest is intended to be utilized for enhancing of LECE of silicon solar cells.

## 2. Experimental

$Ba_4Y_3F_{17}:Yb:Eu$  powders were synthesized by co-precipitation from aqueous nitrate solutions technique as reported earlier [14]. 99.99 wt. % dihydrate potassium fluoride (REACHEM, Russia), 99.99 wt. % yttrium, ytterbium, and europium nitrate hexahydrates, barium nitrate (all reagents from LANHIT, Russia), and double distilled water were used as starting materials without additional purification. Potassium fluoride was preliminarily dried at 350 °C for 3 hours and it was taken with a 50 % excess from stoichiometry. 0.08 M aqueous solutions of barium nitrate and rare earth nitrate were added dropwise to potassium fluoride (0.16 M) with vigorous stirring. Precipitates were washed several times by double distilled water and collected by centrifugation. The resulting precipitates were dried at 45 °C and annealed in a platinum crucible in air at 600 °C for 1 hour. X-ray powder diffraction analysis was performed on a Bruker D8 Advance diffractometer with  $CuK\alpha$  radiation. The TOPAS software ( $R_{wp} < 10$ ) was used for calculation of X-ray coherent scattering domain and unit cell parameters. The morphology, particle size, and composition of the samples were analyzed by a Carl Zeiss NVision 40 scanning electron microscope equipped with an EDX detector.

Raman spectra were captured with a multi-purpose analytical instrument NTEGRA SPECTRA™ (NT-MDT) in epi-configuration. The spectrometer was wavelength calibrated with a silicon wafer by registering a first-order Raman band centered at 520  $cm^{-1}$ . A sensitivity of the spectrometer was as high as ca. 3500 photon counts per 0.1 s provided that we used a 100× objective (N.A. = 0.7), an exit slit of 100  $\mu m$  and a linearly polarized light with the wavelength of 532 nm and the intensity of 5.4  $MW/cm^2$ . The Raman spectra were collected with the EMCCD camera cooled down to -100 °C and registered with spectral resolution of 3  $cm^{-1}$  using a 600 grooves/mm grating.

Photoluminescence was excited by pulsed UV and visible laser radiation from the  $H_2$  Raman shifter cell converting the 266 nm UV radiation from LS2147 laser and/or OPO laser system produced by JV Lotis TII. The pulse duration was 10 ns, repetition rate 10 Hz. The luminescence spectra were registered by a StellarNet EPP2000 portable spectrometer with a spectral resolution of about 0.5 nm. The luminescence kinetics were registered with a MDR-23 monochromator and FEU-100 photomultiplier tube for the UV-visible spectral range and FEU-62 photomultiplier tube for the NIR spectral range and recorded with the 1 GHz 8 bit Rhode-Schwartz oscilloscope. The direct measurements of luminescence quantum yield were performed using the luminescence spectra recorded in a Thorlabs IS200 integrating sphere coupled to a StellarNet EPP2000 spectrometer via an optical fiber. The spectral sensitivity of this system was calibrated using an approach described previously [21].

## 3. Sample characterization

The samples were single-phase according to X-ray powder diffraction after annealing at 600 °C (Fig. 1). The unit cell parameters are in convenience with preliminary data published elsewhere (Table 1) [14, 22].

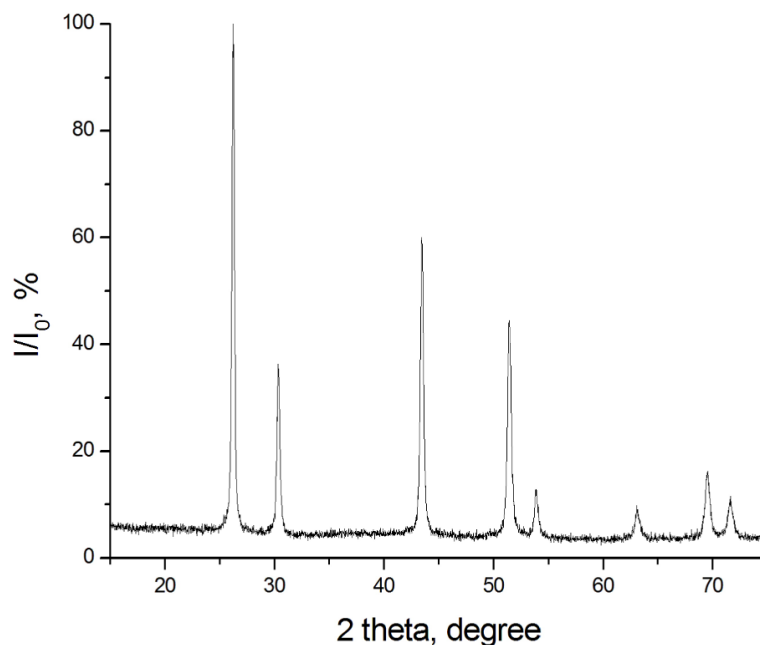


FIG. 1. X-ray powder diffraction for  $Ba_4Y_3F_{17}:Yb(5.0 \text{ mol.}\%): Eu(0.1 \text{ mol.}\%)$  powder after annealing at 600 °C

TABLE 1. Unit cell parameters and X-ray coherent scattering domain for  $\text{Ba}_4\text{Y}_3\text{F}_{17}:\text{Yb}:\text{Eu}$  samples

Nominal composition	$a$ , Å	X-ray coherent scattering domain, nm
$\text{Ba}_4\text{Y}_3\text{F}_{17}:\text{Yb}(1.0 \text{ mol. } \%):\text{Eu}(0.1 \text{ mol. } \%)$	5.9252(2)	$73 \pm 5$
$\text{Ba}_4\text{Y}_3\text{F}_{17}:\text{Yb}(5.0 \text{ mol. } \%):\text{Eu}(0.1 \text{ mol. } \%)$	5.8960(2)	$49 \pm 3$
$\text{Ba}_4\text{Y}_3\text{F}_{17}:\text{Yb}(10.0 \text{ mol. } \%):\text{Eu}(0.1 \text{ mol. } \%)$	5.8793(3)	$75 \pm 11$
$\text{Ba}_4\text{Y}_3\text{F}_{17}:\text{Yb}(1.0 \text{ mol. } \%):\text{Eu}(0.05 \text{ mol. } \%)$	5.8890(3)	$96 \pm 15$
$\text{Ba}_4\text{Y}_3\text{F}_{17}:\text{Yb}(5.0 \text{ mol. } \%):\text{Eu}(0.05 \text{ mol. } \%)$	5.8801(3)	$> 100$
$\text{Ba}_4\text{Y}_3\text{F}_{17}:\text{Yb}(10.0 \text{ mol. } \%):\text{Eu}(0.05 \text{ mol. } \%)$	5.8843(3)	$> 100$

Scanning electron microscopy revealed that the particles were about 100 nm without agglomeration (Fig. 2). The particle sizes well correlated with X-ray coherent scattering domains (Table 1), which means that all particles are single crystalline.

The real compositions were revealed by energy-dispersion analysis (Table 2). The content of the yttrium and barium are close to nominal content. In contrast, the contents of ytterbium and europium are higher than nominal ones, but it is lower than the error of analysis.

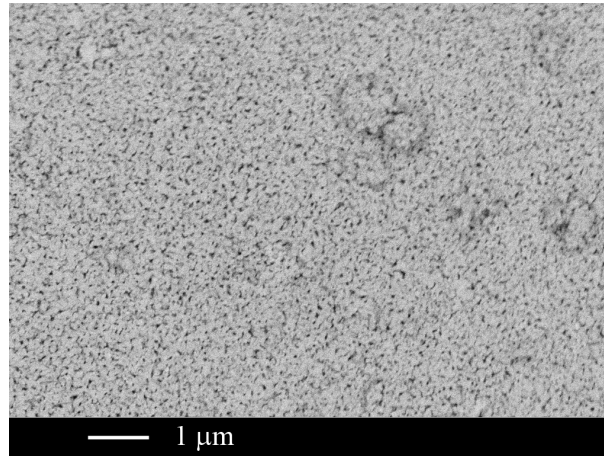


FIG. 2. The typical scanning electron microscopy image for  $\text{Ba}_4\text{Y}_3\text{F}_{17}:\text{Yb}(5.0 \text{ mol. } \%):\text{Eu}(0.1 \text{ mol. } \%)$  powder after annealing at  $600 \text{ }^\circ\text{C}$

TABLE 2. Compositions based on EDX analysis of  $\text{Ba}_4\text{Y}_3\text{F}_{17}:\text{Yb}:\text{Eu}$  samples

Initial nominal compositions	Real chemical compositions from EDX analysis
$\text{Ba}_4\text{Y}_3\text{F}_{17}:\text{Yb}(1.0 \text{ mol. } \%):\text{Eu}(0.1 \text{ mol. } \%)$	$\text{Ba}_{0.638}\text{Y}_{0.344}\text{Yb}_{0.014}\text{Eu}_{0.004}\text{F}_{2.362}$
$\text{Ba}_4\text{Y}_3\text{F}_{17}:\text{Yb}(5.0 \text{ mol. } \%):\text{Eu}(0.1 \text{ mol. } \%)$	$\text{Ba}_{0.568}\text{Y}_{0.364}\text{Yb}_{0.065}\text{Eu}_{0.004}\text{F}_{2.435}$
$\text{Ba}_4\text{Y}_3\text{F}_{17}:\text{Yb}(10.0 \text{ mol. } \%):\text{Eu}(0.1 \text{ mol. } \%)$	$\text{Ba}_{0.585}\text{K}_{0.021}\text{Y}_{0.363}\text{Yb}_{0.138}\text{Eu}_{0.004}\text{F}_{2.706}$
$\text{Ba}_4\text{Y}_3\text{F}_{17}:\text{Yb}(1.0 \text{ mol. } \%):\text{Eu}(0.1 \text{ mol. } \%)$	$\text{Ba}_{0.530}\text{K}_{0.014}\text{Y}_{0.387}\text{Yb}_{0.065}\text{Eu}_{0.003}\text{F}_{2.439}$
$\text{Ba}_4\text{Y}_3\text{F}_{17}:\text{Yb}(10.0 \text{ mol. } \%):\text{Eu}(0.05 \text{ mol. } \%)$	$\text{Ba}_{0.543}\text{Y}_{0.323}\text{Yb}_{0.131}\text{Eu}_{0.003}\text{F}_{2.457}$

The Raman spectrum contains several bands around  $300\text{ cm}^{-1}$  and  $600\text{ cm}^{-1}$ , which is characteristic for fluorides with narrow phonon spectra, see Fig. 3. On the other hand, the Raman spectra tail spreads above  $800\text{ cm}^{-1}$ , which is non-typical for fluorides and may influence on the energy transfer processes.

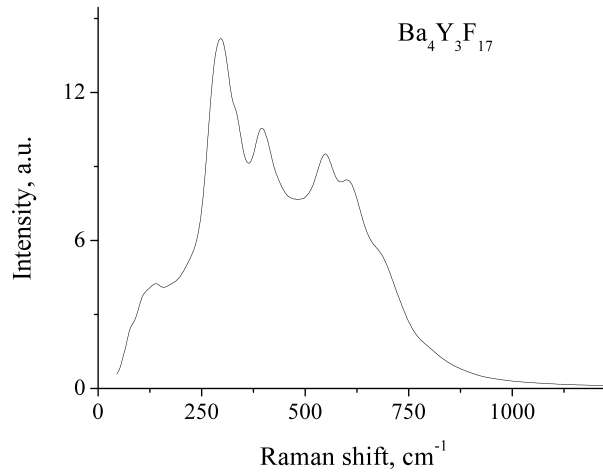


FIG. 3. Raman spectrum of  $Ba_4Y_3F_{17}$  sample

Luminescence of  $Eu^{3+}$  ions can be excited by transitions from the  ${}^7F_0$  ground state to the  ${}^5D_J$  manifolds, in particular, due to  ${}^7F_0 \rightarrow {}^5D_2$  transition located around  $465\text{ nm}$  with relatively large cross-section. The excitation of luminescence is also possible in UV spectral range as the result of transitions to  ${}^5I_J$  and  ${}^5K_J$  manifolds or the charge transfer states (Fig. 4). In order to avoid photodynamic processes initiated under intense UV pumping and following color center formation [23], which can distort the spectral-luminescent properties, excitation was performed at  $296$ ,  $399$  and  $463\text{ nm}$  (transitions  ${}^7F_0 \rightarrow {}^5H_{5,6}$ ,  ${}^5L_6$  and  ${}^5D_2$ , correspondingly) only.

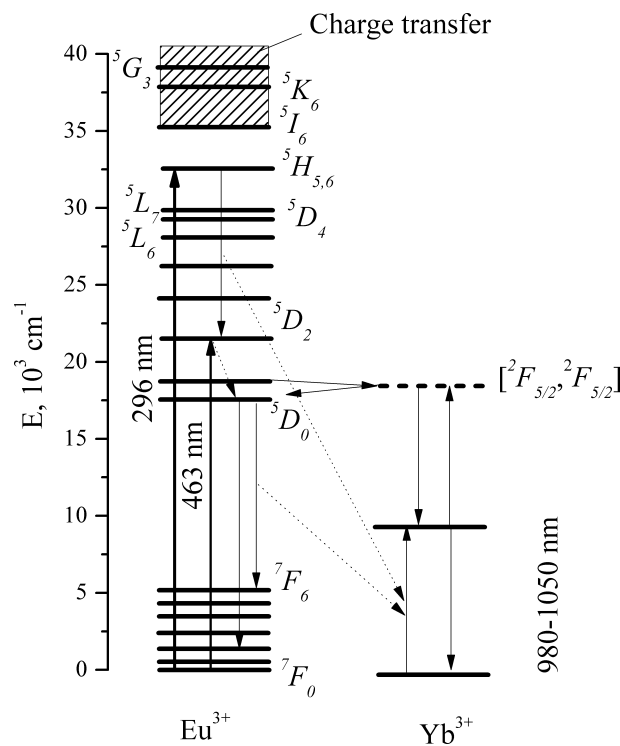


FIG. 4. Energy diagram of  $Eu^{3+}$  and  $Yb^{3+}$  ions and the energy transfer processes from  $Eu^{3+}$  to  $Yb^{3+}$  ions [24]

In the case of double doped samples by  $\text{Eu}^{3+}$  and  $\text{Yb}^{3+}$  ions, the energy gap between  ${}^5\text{H}_{5,6}$  and  ${}^5\text{D}_2$  states of  $\text{Eu}^{3+}$  ions is close to the  ${}^2\text{F}_{7/2}$ - ${}^2\text{F}_{5/2}$  transition energy of  $\text{Yb}^{3+}$  ions. Following the results of [24] the energy transfer from  $\text{Eu}^{3+}$  to  $\text{Yb}^{3+}$  ions may occur through various mechanisms, for example:  ${}^5\text{H}_{5,6}(\text{Eu}^{3+}) + {}^2\text{F}_{7/2}(\text{Yb}^{3+}) \rightarrow {}^5\text{D}_2(\text{Eu}^{3+}) + {}^2\text{F}_{5/2}(\text{Yb}^{3+})$ , or  ${}^5\text{D}_0(\text{Eu}^{3+}) + {}^2\text{F}_{7/2}(\text{Yb}^{3+}) \rightarrow {}^7\text{F}_6(\text{Eu}^{3+}) + {}^2\text{F}_{5/2}(\text{Yb}^{3+})$  as it is illustrated in Fig. 4.

The luminescence spectrum under pulsed excitation at 296 nm consists of  $\text{Eu}^{3+}$  transitions from  ${}^5\text{D}_3$ ,  ${}^5\text{D}_2$ ,  ${}^5\text{D}_1$  and  ${}^5\text{D}_0$  states localized in 400 – 750 nm range, as well as luminescence of  $\text{Yb}^{3+}$  ions  ${}^2\text{F}_{5/2} \rightarrow {}^2\text{F}_{7/2}$ , which is situated around 980 – 1000 nm (Fig. 5). The most intense luminescence bands at 465 nm, 488 nm and 511 nm correspond to  ${}^5\text{D}_2 \rightarrow {}^7\text{F}_{0,2,3}$  transitions, at 526 nm, 538 nm and 557 nm bands – to  ${}^5\text{D}_1 \rightarrow {}^7\text{F}_{0,1,2}$  and at 576 nm, 592 nm, 617 nm and 699 nm – to  ${}^5\text{D}_0 \rightarrow {}^7\text{F}_{0,1,2,4}$  transitions, respectively. The NIR luminescence of  $\text{Yb}^{3+}$  ions is evidence of the energy transfer processes from  $\text{Eu}^{3+}$  to  $\text{Yb}^{3+}$  ions. At the same time, the luminescence of  ${}^2\text{F}_{5/2}$ - ${}^2\text{F}_{7/2}$  of  $\text{Yb}^{3+}$  ions was not detected for the case of excitation at 399 nm or 463 nm.

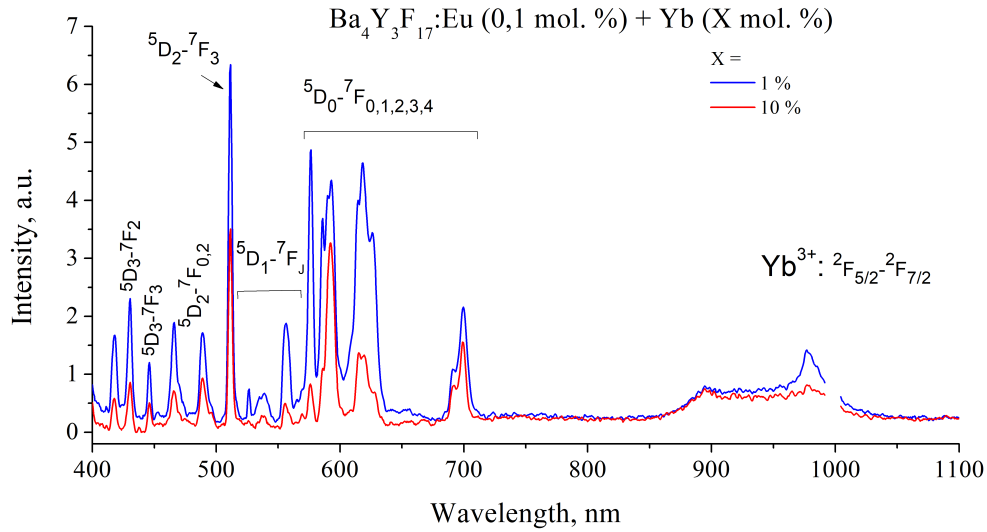


FIG. 5. Typical luminescence spectra of  $\text{Ba}_4\text{Y}_3\text{F}_{17}:\text{Yb}:\text{Eu}$  samples under pulsed excitation at 296 nm

The energy transfer coefficients from  $\text{Eu}^{3+}$  to  $\text{Yb}^{3+}$  were estimated from the luminescence spectra using expression (1):

$$q^E = \frac{\int I^{Yb}(\lambda) d\lambda}{\int (I^{Yb}(\lambda) + I^{Eu}(\lambda)) d\lambda} \times 100 \%, \quad (1)$$

where  $I^{Yb}(\lambda)$  is the luminescence intensity of  $\text{Yb}^{3+}$  and  $I^{Eu}(\lambda)$  is the luminescence intensity of  $\text{Eu}^{3+}$  (Table 3). The increase of doping level leads to some saturation of energy transfer coefficient most probably due to luminescence concentration quenching effect. Thus there should be some optimal content ratio for Yb/Eu ions contents.

TABLE 3. Energy transfer coefficients (%) from  $\text{Eu}^{3+}$  to  $\text{Yb}^{3+}$  in  $\text{Ba}_4\text{Y}_3\text{F}_{17}:\text{Yb}:\text{Eu}$  samples

Eu content, mol. %	Yb content, mol. %		
	1.0	5.0	10.0
0.05	$8 \pm 1$	$5 \pm 1$	$9 \pm 1$
0.10	$11 \pm 1$	$15 \pm 1$	$9 \pm 1$

It is exhibited in fluorescence kinetics. The luminescence decays of  $\text{Ba}_4\text{Y}_3\text{F}_{17}:\text{Yb}^{3+}:\text{Eu}^{3+}$  samples from  ${}^5\text{D}_1$  and  ${}^5\text{D}_0$  states of  $\text{Eu}^{3+}$  at 556 nm and 617 nm, correspondingly, and from  ${}^2\text{F}_{5/2}$  of  $\text{Yb}^{3+}$  ion (at 1020 nm) were investigated under the excitation at 296 nm (Figs. 6 and 7, respectively). The kinetics from  ${}^5\text{D}_1$  state (Fig. 6a) exhibit the long lasting raise (few ms for  $\text{Ba}_4\text{Y}_3\text{F}_{17}:\text{Eu}^{3+}$  (0.1 mol. %)), which is evidence for cross-relaxation effects between

manifolds of  $Eu^{3+}$  ions [22]. However, the lifetime of  ${}^5D_1$  state is weakly dependent on  $Yb^{3+}$  ions' doping level. The luminescence decay from  ${}^5D_0$  state of  $Eu^{3+}$  ions is more complicated and consists of fast and slow components. The contribution of the last one grows with a simultaneous increase of  $Yb^{3+}$  content, which can be attributed to reverse energy transfer from  $Yb^{3+}$  to  $Eu^{3+}$  via cooperative processes [25].

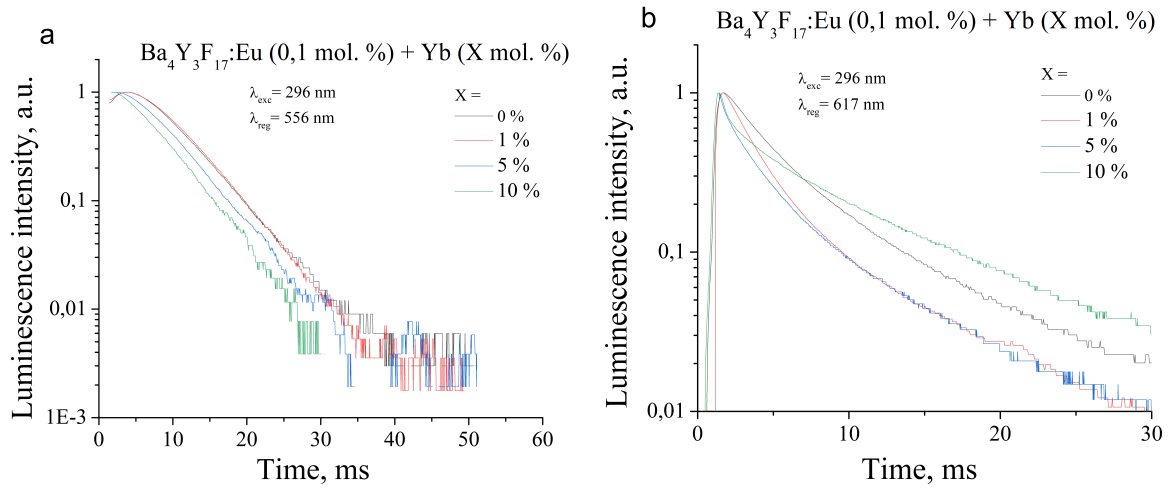


FIG. 6. Luminescence decays of  $Ba_4Y_3F_{17}:Eu(0.1 \text{ mol.}\%):Yb(x \text{ mol.}\%)$ ,  $x = 0, 1.0, 5.0, 10.0$  samples at 556 nm (from  ${}^5D_1$  state) (a) and 617 nm (from  ${}^5D_0$ ) (b) under 296 nm excitation

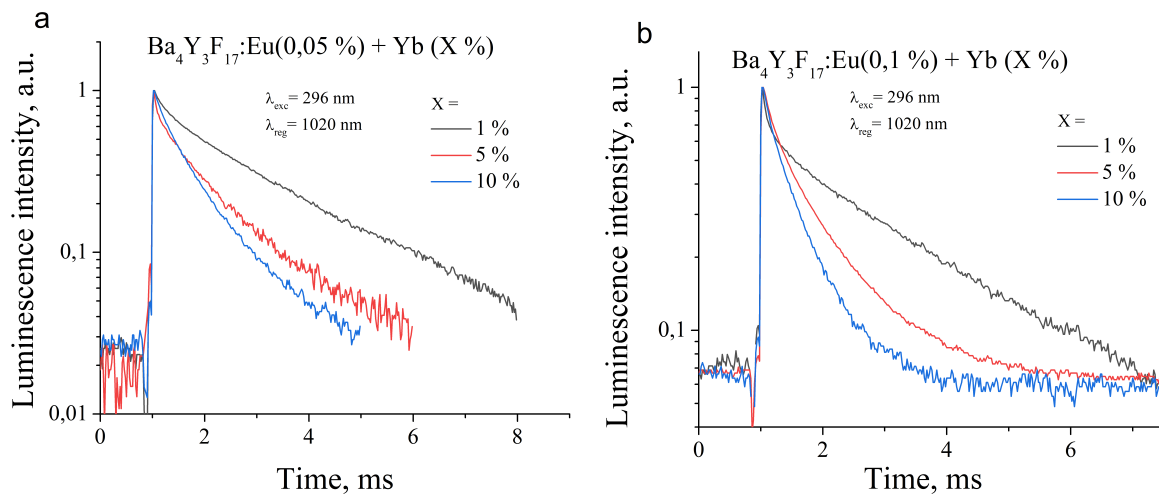


FIG. 7. Luminescence decay kinetics of  $Ba_4Y_3F_{17}:Yb:Eu$  samples at 1020 nm upon 296 nm excitation

The luminescence decays of  $Yb^{3+}$  ions registered at 1020 nm under excitation at 296 nm are not exponential too, and look faster with the increase of  $Yb^{3+}$  ions content. It also proves the reverse energy transfer processes from two excited  $Yb^{3+}$  ( ${}^2F_{5/2}$ ) to  ${}^5D_1$  manifold of  $Eu^{3+}$  ions.

Since the dependence of the luminescence decay of  $Eu^{3+}$  ions at 617 nm differs from the exponential law, the lifetimes were estimated as the average ones according to the formula (2):

$$t_{avg} = \frac{\int t \cdot I(t) dt}{\int I(t) dt}, \quad (2)$$

where  $I(t)$  is dependence of luminescence intensity on time,  $t$  – time. The results of calculation are presented in Table 4.

The average luminescence lifetimes of  ${}^5D_1$  manifold of  $Eu^{3+}$  ions decreases with increasing  $Yb^{3+}$  ions concentration, while the lifetimes assumed to  ${}^5D_0$  manifold increases. This suggests that energy transfer from  $Eu^{3+}$

TABLE 4. Average luminescence lifetimes of  $^5D_0$ ,  $^5D_1$  of  $Eu^{3+}$  and  $^2F_{5/2}$  of  $Yb^{3+}$  ions in  $Ba_4Y_3F_{17}:Eu(0.1 \text{ mol.}\%):Yb(x \text{ mol.}\%)$   $x = 0, 1.0, 5.0, 10.0$  samples under excitation at 296 nm

Registration wavelengths	617 nm	556 nm	1020 nm	
	(from $^5D_0$ )	(from $^5D_1$ )	(from $^2F_{5/2}$ )	
Eu content, mol.%	Eu = 0.10	Eu = 0.10	Eu = 0.05	Eu = 0.10
Yb = 0	$3.0 \pm 0.1 \text{ ms}$	$10.3 \pm 0.1 \text{ ms}$	—	—
Yb = 1.0	$2.2 \pm 0.1 \text{ ms}$	$10.2 \pm 0.1 \text{ ms}$	$2.0 \pm 0.1 \text{ ms}$	$2.0 \pm 0.1 \text{ ms}$
Yb = 5.0	$5.6 \pm 0.1 \text{ ms}$	$8.4 \pm 0.1 \text{ ms}$	$0.9 \pm 0.1 \text{ ms}$	$0.8 \pm 0.1 \text{ ms}$
Yb = 10.0	$8.8 \pm 0.1 \text{ ms}$	$7.3 \pm 0.1 \text{ ms}$	$0.7 \pm 0.1 \text{ ms}$	$0.5 \pm 0.1 \text{ ms}$

to  $Yb^{3+}$  ions occurs from higher-lying states than the  $^5D_0$  one, which can cause a low quantum yield of ytterbium down-conversion luminescence, since these states are characterized by shorter lifetimes. Therefore, taking into account the absence of the  $Eu^{3+}-Yb^{3+}$  energy transfer under excitation at 399 nm and 465 nm and despite the fact of existing of luminescence from  $^5D_3$  state of  $Eu^{3+}$ , the most probable mechanism is  $^5H_{5,6}(Eu^{3+})-^2F_{7/2}(Yb^{3+}) \rightarrow ^5D_2(Eu^{3+})-^2F_{5/2}(Yb^{3+})$  energy transfer process.

Finally, using the integrating sphere, the quantum yield of  $Yb^{3+}$  luminescence was measured under the 296 nm excitation (Table 5).

TABLE 5. Quantum yields for  $Ba_4Y_3F_{17}:Yb:Eu$  samples at 296 nm excitation

Eu content mol, %	Yb content, mol, %		
	1.0	5.0	10.0
0.05	$0.4 \pm 0.05 \%$	$0.2 \pm 0.05 \%$	$0.3 \pm 0.05 \%$
0.10	$0.3 \pm 0.05 \%$	$0.4 \pm 0.05 \%$	$0.2 \pm 0.05 \%$

The maximum quantum yields for  $Ba_4Y_3F_{17}$  samples were recorded for the  $Eu/Yb$  ratios of 0.1/1 and 0.1/10.0 and amounted to 0.4 %. It is obvious that competition of mutually oppositely directed energy transfer processes has determined such a small value of quantum yield of down-conversion luminescence of  $Yb^{3+}$  ions in the studied samples.

#### 4. Conclusions

The single-phase solid solutions  $Ba_4Y_3F_{17}:Yb:Eu$  with fluorite-type structure were synthesized by co-precipitation from aqueous solution technique. The average particle size was approximately 100 nm without agglomeration, which correlated with X-ray coherent scattering domains. The luminescence spectra from all  $^5D_J$  manifold of  $Eu^{3+}$  ions were observed under irradiation at various wavelengths, whereas the sensitized down-conversion luminescence of  $Yb^{3+}$  ions, which was detected for the 296 nm excitation only, was not observed for resonant excitation to  $^5D_J$  states of  $Eu^{3+}$ . Moreover, the reverse cooperative energy transfer from a pair of  $Yb^{3+}$  ions in the excited  $^2F_{5/2}$  state to  $^5D_0$  state of  $Eu^{3+}$  ions was observed. The quantum yield of  $Yb^{3+}$  down-conversion luminescence was measured using the integrating sphere. The maximal value was 0.4 % for the  $Eu/Yb$  ratios of 0.1/1.0 and 0.1/10.0, which appears because of competition of mutually opposite directed energy transfer processes between  $Eu^{3+}$  and  $Yb^{3+}$  ions.

#### Acknowledgements

This work was supported by the Russian Science Foundation, grant 17-73-20352. Authors thank to M. N. Mayakova for valuable help in sample preparation.

## References

- [1] Weber E.R. Photovoltaics moving into the terawatt age. *Proc. SPIE, Next Generation Technologies for Solar Energy Conversion VIII*, 2017, **10368**, 1036803.
- [2] Lehr J., Langenhorst M., et al. Energy yield of bifacial textured perovskite/silicon tandem photovoltaic modules. *Solar Energy Materials and Solar Cells*, 2020, **208**, 110367 P. 1–9.
- [3] Im J.-H., Lee C.-R., et al. 6.5 % efficient perovskite quantum-dot-sensitized solar cell. *Nanoscale*, 2011, **3**, P. 4088–4093.
- [4] Han G., Zhang S., et al. Towards high efficiency thin film solar cells. *Prog. Mater. Sci.*, 2017, **87**, P. 246–291.
- [5] Huang X., Han S., Huang W., Liu X., Enhancing solar cell efficiency: the search for luminescent materials as spectral converters. *Chem. Soc. Rev.*, 2013, **42**, P. 173–201.
- [6] Moraitis P., Schropp R.E.I., Sark W.G.J.H.M. Nanoparticles for luminescent solar concentrators – a review. *Opt. Mater.*, 2018, **84**, P. 636–645.
- [7] Green M.A., Bremner S.P. Energy conversion approaches and materials for high efficiency photovoltaics. *Nat. Mater.*, 2017, **16**, P. 23–34.
- [8] Trupke T., Green M.A., Würfel P. Improving solar cell efficiencies by down-conversion of high-energy photons. *J. Appl. Phys.*, 2002, **92**, P. 1668–1674.
- [9] Yu P., Yao Y., et al. Effects of plasmonic metal core-dielectric shell nanoparticles on the broadband light absorption enhancement in thin film solar cells. *Sci. Rep.*, 2017, **7**, P. 7696.
- [10] Fang D., Zhang X., et al. Application of bidirectional (up and down)-conversion luminescence material ( $GdBO_3:Yb^{3+}/Tb^{3+}$ ) in  $CdSe_{0.4}S_{0.6}$  quantum dot-sensitized solar cells. *Opt. Mater.*, 2019, **88**, P. 80–90.
- [11] Gu H., Wang J., et al. The core-shell-structured  $NaYF_4:Er^{3+}, Yb^{3+}@NaYF_4:Eu^{3+}$  nanocrystals as dual-mode and multifunctional luminescent mechanism for high-performance dye-sensitized solar cells. *Mater. Res. Bull.*, 2018, **108**, P. 219–225.
- [12] Buarque J.M.M., Manzani D., et al.  $SiO_2-TiO_2$  doped with  $Er^{3+}/Yb^{3+}/Eu^{3+}$  photoluminescent material: a spectroscopy and structural study about potential application for improvement of the efficiency on solar cells. *Mater. Res. Bull.*, 2018, **107**, P. 295–307.
- [13] Rajesh D., Dousti M.R., Amjad R.J., Camargo A.S.S. Quantum cutting and upconversion investigations in  $Pr^{3+}/Yb^{3+}$  co-doped oxyfluorotellurite glasses. *J. Non-Cryst. Solids*, 2016, **450**, P. 149–155.
- [14] Kuznetsov S.V., Nizamutdinov A.S., et al. Synthesis and down-conversion luminescence of  $Ba_4Y_3F_{17}:Yb:Pr$  solid solutions for photonics. *Nanosystems: Physics, Chemistry, Mathematics*, 2019, **10**, P. 190–198.
- [15] Li T., Li Y., et al. Novel  $Ba(Gd_{1-x}Y_x)_{0.78}F_5: 20 \text{ mol } \% Yb^{3+}, 2 \text{ mol } \% Tm^{3+}$  ( $0 < x < 1.0$ ) solid solution nanocrystals: A facile hydrothermal controlled synthesis, enhanced upconversion luminescent and paramagnetic properties. *J. Alloys Comp.*, 2018, **740**, P. 1204–1214.
- [16] Karbowski M., Cichos J. Does  $BaYF_5$  nanocrystals exist? The  $BaF_2-YF_3$  solid solution revisited using photoluminescence spectroscopy. *Journal of Alloys and Compounds*, 2016, **673**, P. 258–264.
- [17] Fedorov P.P., Kuznetsov S.V., et al. Coprecipitation from aqueous solutions to prepare binary fluorides. *Russian J. of Inorg. Chem.*, 2011, **56**, P. 1525–1531.
- [18] Kuznetsov S.V., Proydakova V.Yu., et al. Synthesis and quantum yield investigations of the  $Sr_{1-x-y}Pr_xYb_yF_{2+x+y}$  luminophores for photonics. *Nanosystems: Physics, Chemistry, Mathematics*, 2018, **9**, P. 663–668.
- [19] Kuznetsov S.V., Morozov O.A., et al.  $Ca_{1-x-y}Yb_xPr_yF_{2+x+y}$  solid solution powders as a promising materials for crystalline silicon solar energetics. *Nanosystems: Physics, Chemistry, Mathematics*, 2018, **9**, P. 259–265.
- [20] Kuznetsov S.V., Nizamutdinov A.S., et al. Synthesis and Luminescence of  $Sr_{1-x-y}Yb_xEu_yF_{2+x+y}$ . Solid Solutions for Photonics. *Inorganic Materials*, 2019, **55**, P. 1031–1038.
- [21] Yasyrkina D.S., Kuznetsov S.V., et al. Dependence of quantum yield of up-conversion luminescence on the composition of fluorite-type solid solution  $NaY_{1-x-y}Yb_xEr_yF_4$ . *Nanosystems: Physics, Chemistry, Mathematics*, 2013, **4**, P. 648–656.
- [22] Kuznetsov S.V., Fedorov P.P., et al. Synthesis of  $Ba_4R_3F_{17}$  (R stands for Rare-Earth Elements) Powders and Transparent Compacts on Their Base. *Russian Journal of Inorganic Chemistry*, 2010, **55**, P. 484–493.
- [23] Semashko V.V. Problems in searching for new solid-state UV- and VUV active media: the role of photodynamic processes. *Phys. of Solid State*, 2005, **47**, P. 1507–1511.
- [24] Van der Voort D., Dirksen G.J., Blasse G. Luminescence study of  $Eu^{3+}-O^{2-}$  associates in fluorides:  $CaF_2$ ,  $RbCdF_3$ , and  $RbCaF_3$ . *J. Phys. Chem. Solids*, 1992, **53**, P. 219–225.
- [25] Dwivedi Y., Zilio S.C. Infrared cascade and cooperative multicolor upconversion emissions in  $Y_8V_2O_{17}:Eu:Yb$  nanophosphors. *Opt. Express*, 2013, **21**, P. 4717–4727.